Taylor & Francis
Taylor & Francis Group

Science and Technology of Advanced Materials: Methods

ISSN: (Print) (Online) Journal homepage: https://www.tandfonline.com/loi/tstm20

Comprehensive elemental screening of solid-solution copper alloys

Kenji Yamaguchi, Takuya Ishigaki, Yuki Inoue, Shuhei Arisawa, Hirotaka Matsunoshita, Yuki Ito, Hiroyuki Mori, Ken'ichiro Suehiro, Kazunari Maki, Kenji Nagata & Masahiko Demura

To cite this article: Kenji Yamaguchi, Takuya Ishigaki, Yuki Inoue, Shuhei Arisawa, Hirotaka Matsunoshita, Yuki Ito, Hiroyuki Mori, Ken'ichiro Suehiro, Kazunari Maki, Kenji Nagata & Masahiko Demura (2023) Comprehensive elemental screening of solid-solution copper alloys, Science and Technology of Advanced Materials: Methods, 3:1, 2250704, DOI: 10.1080/27660400.2023.2250704

To link to this article: https://doi.org/10.1080/27660400.2023.2250704

SCIENCE AND TECHNOLOGY OF ADVANCED MATERIALS: METHODS
2023, VOL. 3, NO. 1, 2250704
https://doi.org/10.1080/27660400.2023.2250704

Comprehensive elemental screening of solid-solution copper alloys

Kenji Yamaguchi[a], Takuya Ishigaki[a], Yuki Inoue[a], Shuhei Arisawa[b], Hirotaka Matsunoshita[b], Yuki Ito[b], Hiroyuki Mori[b], Ken'ichiro Suehiro[b], Kazunari Maki[b], Kenji Nagata[c] and Masahiko Demura[c]

[a]Innovation Center, Mitsubishi Materials Corporation, Naka, Japan; [b]Kitamoto-branch, Innovation Center, Mitsubishi Materials Corporation, Kitamoto, Japan; [c]Research and Services Division of Materials Data and Integrated System, National Institute for Materials Science, Tsukuba, Japan

ABSTRACT

Significantly improving the balance between the mechanical strength and electrical conductivity of solid-solution copper alloys is considered difficult. In this study, a comprehensive elemental screening framework is proposed to predict the solid-solution strengthening and electrical resistivity of copper alloys. Electrical resistivities are predicted by first-principles calculations, and a high degree of accuracy is obtained. Two models are considered to predict the solid-solution strengthening. One of them uses the generalized critical resolved shear stress formula and provides a reasonable accuracy for a testing set of our experimental data. The other model (using the first model as a feature with elemental features) has a high prediction performance for the testing set. Combining the predicted electrical resistivity and solid-solution strengthening, we establish a figure-of-merit formula for the comprehensive elemental screening. The formula provides reasonable results using the two models. The models predicted the known Cu–Ag (Cd, In, Mg) as high-performance copper alloys. All solute elements, H to Rn, including hypothetical copper alloys are ranked, and the less studied Cu–Au, –Hg, and –Tl are predicted to be high-performance structures. From economic, environmental, and healthcare perspectives, Cu–Mg is an appropriate choice according to the results.

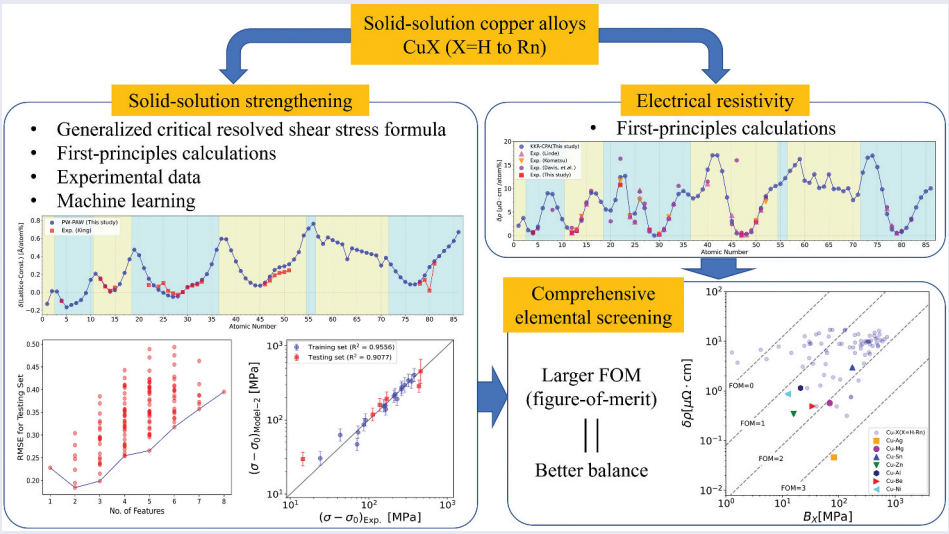

ARTICLE HISTORY
Received 3 July 2023
Revised 1 August 2023
Accepted 17 August 2023

KEYWORDS
Alloy design; copper alloys; mechanical properties; electrical resistivity/conductivity; density functional theory (DFT); modelling

IMPACT STATEMENT

For designing the balance between mechanical strength and electrical conductivity of solid-solution copper alloys, a figure-of-merit formula using theoretical formula, first-principles calculations, experimental data, and machine learning is established.

1. Introduction

Various copper alloys are widely used in the industry owing to their unique combinations of electrical, mechanical, and physical properties [1]. Among them, solid-solution (SS) copper alloys such as brass and phosphor bronze are major industrial materials because of their simple production processes, low costs, and adequate balance between the mechanical strength and electrical conductivity (EC). Although we have shown that supersaturation with Mg provides an

CONTACT Kenji Yamaguchi kyam@mmc.co.jp Innovation Center, Mitsubishi Materials Corporation, 1002-14, Mukohyama, Naka, Ibaraki 311-0102, Japan

Supplemental data for this article can be accessed online at https://doi.org/10.1080/27660400.2023.2250704.

excellent balance [2,3] and has already been commercialized as a high-performance copper alloy product, a better balance between the mechanical strength and EC might be realized by other unconsidered SS elements.

Recently, Liu et al. reviewed applications of a machine learning (ML)-assisted alloy design to explore the design freedom with diverse materials [4]; they presented two previous studies on copper alloys [5,6]. In Ref. [5], two back-propagation neural network models to map the relationship between compositions and properties of tensile strength and EC are constructed with data of Cu–Fe–P-, Cu–Ni–Si-, and Cu–Cr–Zr-based alloys, including SS, precipitation, and deformation-strengthened samples. In Ref. [6], an ML model for selected alloy elements to enhance SS-strengthened conductive copper alloys has been constructed. The model predicted that the optimal element is indium, and the experimental results of Cu–In alloys showed significant improvements in the combined ultimate tensile strength (UTS) and EC. Although the key elemental features of the ML model, such as electronegativity for UTS, could be universally applied to design various alloys, the predicted properties of Cu–Ag, which have similar electronegativities of 1.90 and 1.93, respectively, have not been presented, and further predictive ability has not been indicated. To the best of our knowledge, no universally applicable model for supersaturated SS copper alloys with various elements has been reported to predict the balance between the mechanical strength and EC. In recent years, several projects on the preparation of large first-principles calculations databases have been carried out to predict how new materials, both real and hypothetical, can be applied; examples of such projects are Materials Project [7], AFLOW [8], and NOMAD [9]. Elastic tensor components for the prediction of mechanical properties are set for 7,108 and 5,650 materials in Materials Project [7] and AFLOW [8], respectively, while only seven species of cubic Cu3X1 (X = N, Al, Sc, Pd, Hf, Pt, and Au) are in Materials Project [7]. SS strengthening (SSS) originates from interactions between solute atoms and dislocations, as described by Fleischer [10] and Labusch [11]. The strengthening effects can be evaluated using the changes in the solute alloy factors of lattice constant and shear modulus. In principle, we can evaluate the effects by first-principles calculations; however, insufficient data are presented in the previous projects, and we could not find other comprehensive studies. Furthermore, no electrical resistivity (ER) was set to evaluate the EC properties in the projects on large first-principles calculations databases.

In this paper, we propose a comprehensive elemental screening model for copper SS alloys to design the balance between SSS and ER. The ERs were directly obtained via first-principles calculations, and SSS effects were evaluated using modelling, first-principles calculations, and ML. For the prediction of SSS and ER of copper alloys, comparisons were made between experimental results in the literature and those in this study. We limited our search to binary copper alloys, because we considered it undesirable to increase the number of elements while preparing for the establishment of the copper recycling technology, which is still under development [12].

2. Methods

2.1. Framework

Our proposed framework for the comprehensive elemental screening model is depicted in Figure 1. Experimental data were prepared with 0.2% yield strength and ER measurements [2]. Additional experiments were conducted for the testing set for verification. We used the generalized critical resolved shear stress formula [13,14] as an SSS model (Model-1) and determined its parameters using first-principles calculations and fitting to experimental data. Model-1 is described by [13,14]

$$\sigma - \sigma_0 = A \cdot G \cdot \varepsilon^p \cdot x^q \tag{1}$$

where $\sigma - \sigma_0$ is the increase in the 0.2% yield strength from that of pure Cu, G is the shear modulus, x is the solute content in molar fractions, ε is a mismatch parameter, and A, p, and q are constants. The mismatch parameter ε is expressed by the elastic misfit ε_G and atomic size misfit ε_l:

$$\varepsilon = \sqrt{(\varepsilon_G)^2 + (\alpha \cdot \varepsilon_l)^2} \tag{2}$$

where the parameter α varies with the character of dislocations: $3 < \alpha < 16$ for screw dislocations and $\alpha > 16$ for edge dislocations [13,14]. The elastic misfit ε_G and atomic size misfit ε_l are

$$\varepsilon_G = \frac{\delta_G}{1 + 0.5|\delta_G|}; \delta_G = \frac{1}{G} \cdot \frac{dG}{dx}; \varepsilon_l = \frac{1}{l} \cdot \frac{dl}{dx} \tag{3}$$

where l is the lattice constant of the cubic alloy. In this study, the parameters A, p, q, and α were determined by numerical fitting between the experimental data of 0.2% yield strength and Equation (1), with the G and l values obtained via first-principles calculations. To improve the predictive ability for SSS, ML modelling (Model-2) was carried out using elemental features and Model-1 as a feature. The additional experimental data were used to validate both Model-1 and Model-2. The ERs were directly obtained using first-principles calculations. The results show a good agreement of the experimental values in the literature and those in this study. Therefore, we did not perform further ML

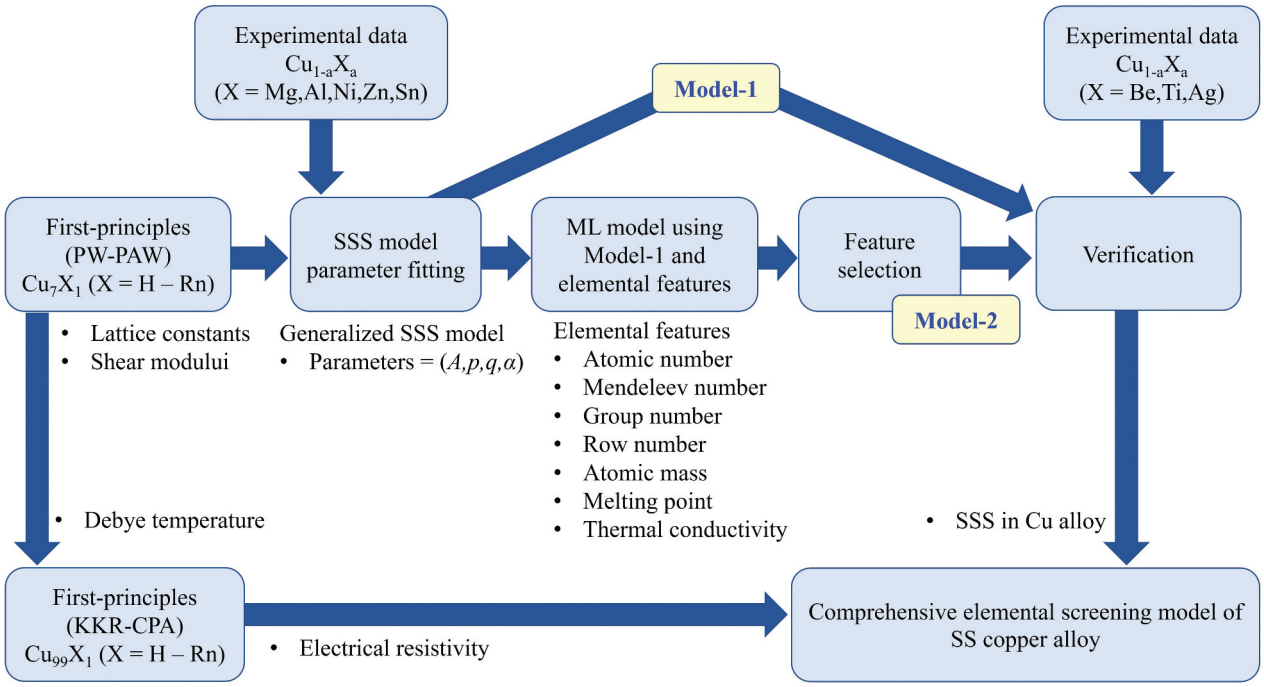

Figure 1. Framework of the comprehensive elemental screening of SS copper alloys. For SSS modelling, lattice constants and shear moduli calculated using the plane-wave projector augmented wave (PW-PAW) method are used. ERs are evaluated via the Korringa–Kohn–Rostoker coherent-potential approximation (KKR-CPA) with the Kubo–Greenwood linear response formalism. Finite-temperature effects are calculated using Debye temperatures estimated by elastic tensor components of PW-PAW results.

modelling for ER. A comprehensive elemental screening model for copper SS alloys was then obtained with the generalized SSS model with/without the correction by ML and calculated ER.

2.2. Experimental data

The preparation procedure of the experimental alloy was the same as that in our previous study [2]. The measured 0.2% yield strengths were used to represent SSS. ERs were obtained from specific resistance measurements via the four-terminal method at room temperature. For the training set for the fitting of Equation (1) and training of the ML model, we used 19 data points: pure Cu, $Cu_{100-x}Mg_x$ (x = 0.7, 2, 3, 4, 5, and 6 atom%), $Cu_{100-x}Al_x$ (x = 4, 8, and 12 atom%), $Cu_{100-x}Zn_x$ (x = 8, 13, and 20 atom%), $Cu_{100-x}Sn_x$ (x = 0.4, 1, 2, and 3 atom%), and $Cu_{100-x}Ni_x$ (x = 3 and 6 atom%). For the testing set for the validation of the models, we used six data points: $Cu_{100-x}Be_x$ (x = 12 atom%), $Cu_{100-x}Ti_x$ (x = 0.5 and 5 atom%), and $Cu_{100-x}Ag_x$ (x = 2, 3, and 4 atom%). These elements of the training set were selected because they are often used in practical applications. The three elements for the testing set (hold out) were selected for the following reasons. Be was selected because it is the lightest element among the experimentally considered elements and provides a high strength. Ti was selected because it has a high solid solubility among the transition metals and was expected to have a high strength. Ag was selected because some of its elemental features are similar to those of Cu, and it was expected to provide a high performance.

2.3. First-principles calculations

In cubic Cu_7X_1 (X = H – Rn), the crystal structures are constructed by a $2 \times 2 \times 2$ structure of the primitive cell of the face-centered cubic copper, and one of the eight sites is substituted by X. The optimized lattice constants and elastic tensor components of Cu_7X_1 were evaluated using first-principles calculations, with a plane-wave basis set with the PW-PAW method [15] based on the density functional theory under the generalized gradient approximation with the Perdew – Burke–Ernzerhof (PBE) exchange-correlation functional [16]. We performed structural optimizations and evaluation of the elastic tensor components using the first-principles calculations code Vienna Ab Initio Simulation Package (VASP; version 5.4) [17–21] with a PW cutoff energy of 500 eV, *k*-point sampling within 0.09 $Å^{-1}$, and convergence criterion for ionic relaxations of 0.001 eV/Å. Elastic properties were calculated using the strain values of −0.01, 0, and + 0.01 to cancel the 3rd order anharmonic effects. By this procedure, obtained elastic constants of copper show good agreement with that of previous work as shown in Table S1. Bulk (*B*) and shear (*G*) moduli were evaluated by arithmetic means, i.e. with the Voight–Reuss–Hill approximation [22]. Using the mass density *m*, the longitudinal and transverse

sound velocities can be expressed as $C_L = \sqrt{\{B + (4/3)G\}/m}$ and $C_T = \sqrt{G/m}$, respectively. In the Debye model, the average sound velocity C_D is

$$\frac{3}{{C_D}^3} = \frac{1}{{C_L}^3} + \frac{2}{{C_T}^3}, \tag{4}$$

while the Debye temperature is

$$\theta_D = \frac{h}{2\pi k_B}\left(\frac{6\pi^2 N}{V}\right)^{1/3} C_D, \tag{5}$$

where h is the Planck constant, k_B is the Boltzmann constant, and N atoms exist in a volume of V. The misfits of Equation (3) were evaluated by variation with pure Cu within the Vegard's law.

$$\begin{aligned} \varepsilon_G \cong \varepsilon_G(X) &\equiv \frac{\delta_{G0}}{1 + 0.5|\delta_{G0}|}; \\ \delta_{G0} &\equiv \frac{1}{G_{Cu}} \cdot \frac{G_{CuX} - G_{Cu}}{0.125}; \\ \varepsilon_l \cong \varepsilon_l(X) &\equiv \frac{1}{l_{Cu}} \cdot \frac{l_{CuX} - l_{Cu}}{0.125} \end{aligned} \tag{6}$$

where G_{Cu} and G_{CuX} are the calculated share moduli of pure Cu and Cu_7X_1, respectively, l_{Cu} and l_{CuX} are the calculated lattice constants of pure Cu and Cu_7X_1, respectively, and ε_G (X) and ε_l (X) are the molar-fraction-independent elastic misfit and atomic size misfit of the solute element X (X = H – Rn), respectively. The calculated atomic size misfits (times l_{Cu}) are in good agreement with the experimentally obtained King's linear-size factors [23] without Hg, as depicted in Figure 2. Throughout this paper, we use the calculated atomic size misfits.

The ERs were calculated using the KKR-CPA [24–26] method with the PBE functional [16] for the completely random substitutional SS $Cu_{99}X_1$ (X = H – Rn). We performed the ER calculations using the version 7.7.3 of the Munich spin-polarized relativistic KKR code [27,28] with the fully relativistic mode. The angular momentum expansion of the basis has a maximum l-value of 3 and 4 for the elements without and with lanthanides, respectively. The energy path under the Fermi level is in the range of approximately 15 eV for the self-consistent field (SCF) calculations. The k-point sampling number in the Brillouin zone is set to 2,500. For some hard-to-converge elements of lanthanides, the number was set to 25,000 for the SCF calculations. For resistivity calculations, 100,000 k-points were used. The ER calculations were performed using the Kubo-Greenwood linear response formalism with vertex corrections [29]. Scattering effects at 300 K with phonons of Debye model are included for calculating ER [30] (for more details, please refer to Supplementary Information 1). The Debye temperatures were used for the interpolation of Equation (5) with pure Cu and Cu_7X_1 (X = H – Rn) VASP calculations. In the calculations, the lattice constants of $Cu_{99}X_1$ (X = H – Rn) were fixed at 3.6342 Å, which is the optimized VASP value of pure copper by our group and is slightly larger than the experimental value of 3.6147 Å. This originated from the well-known property of the PBE method of overestimation of lattice constants [31].

2.4. ML for SSS

We employed an ML model of Gaussian process regression (GPR) with a kernel that is the product of constant and squared exponential kernels plus white noise kernel. Hyperparameters of the kernel were optimized with the training set. We used seven elemental features from the package of pymatgen [32], including mean values of the group number, row number, block number, atomic mass, Mendeleev number, thermal conductivity, and melting point. The other features of pymatgen were not used because they were not available for all elements of H to Rn. In addition, Model-1 as a feature was used for the entire ML model in this study. Elemental features were selected with the minimum condition of root mean square error (RMSE). The predictive performance of models was evaluated by the hold-out method using testing data set. The model training and testing

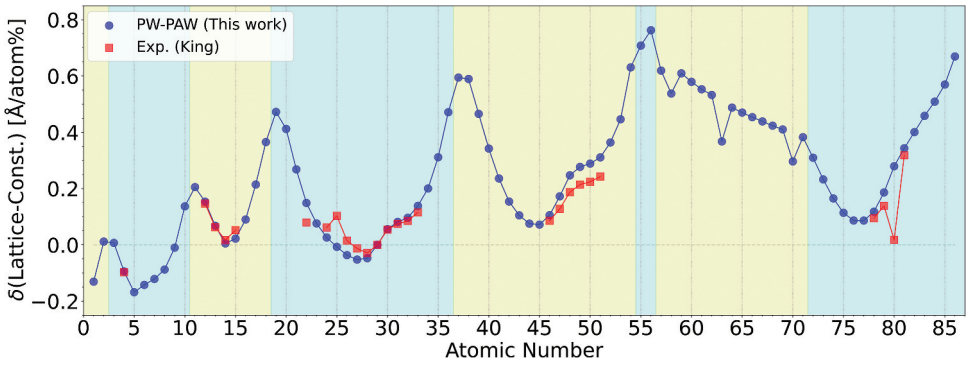

Figure 2. Deviations of the lattice constants of SS copper alloys by each element. The PW-PAW results were obtained using first-principles calculations in this study, and 'Exp. (King)' are obtained by the experimental values of King's linear-size factors [23].

were set up and performed using the scikit-learn version 0.24.2 [33] and matminer version 0.7.3 [34].

3. Results and discussion

3.1. Electrical resistivity

The calculated ER increases of the completely random substitutional SS $Cu_{99}X_1$ (X = H – Rn) relative to the values for pure Cu are

$$\rho - \rho_0 = \delta\rho(X) \cdot x \tag{7}$$

which are shown in Figure 3(a), comparing experimental results from literature [1,35,36] and this study. The molar fraction dependence of nonlinear effects is omitted in Equation (7) and the experimental results. Our calculated results show good agreement with the experimental results, as shown in Figure 3(b), with a coefficient of determination of R2 > 0.91 without the Cu-Pd resistivity results reported by Davis et al. [1]. The Cu-Pd resistivity obtained by Linde [35] is also in good agreement with our calculation. Therefore, we considered the Cu-Pd resistivity results reported by Davis et al. [1] as outlier as shown in Figure 3(b). In this study, we used the calculated resistivity for the comprehensive elemental screening.

3.2. Model-1 for SSS

According to Equations (1–3, 6), Model-1 for SSS is expressed as

$$\text{Model-1} \equiv \text{A} \cdot G_{Cu} \cdot \varepsilon(X)^p \cdot x^q \equiv B_X \cdot x^q \tag{8}$$

where $\varepsilon(X) \equiv \sqrt{\{\varepsilon_G(X)\}^2 + \{\alpha \cdot \varepsilon_l(X)\}^2}$ and $B_X \equiv \text{A} \cdot G_{\text{Cu}} \cdot \varepsilon(\text{X})^p$ are defined as misfit factor and SSS factor for the solute element X (X = H – Rn), respectively. Optimal parameters of Model-1, A, p, q, and α, are obtained by fitting with the 19 data points as a training set; the results are listed in Table 1. The obtained p and q show the same order as that of the theoretical model [10,11,13,14]. The large α implies that only the atomic size misfit contributes to the SSS enhancement caused by the interaction between edge dislocations and the solute atom [13,14]. As shown in Figure 4(a), not only the training set, but also the testing set of six data is well predicted by Model-1 with a coefficient of determination of $R^2 > 0.8$.

3.3. Model-2: ML for SSS

We employed an ML model of GPR as described in 2.4. We define the target as

$$f(\mathbb{R}) \equiv \log_{10}(\sigma - \sigma_0)_{\text{EXP.}} \tag{9}$$

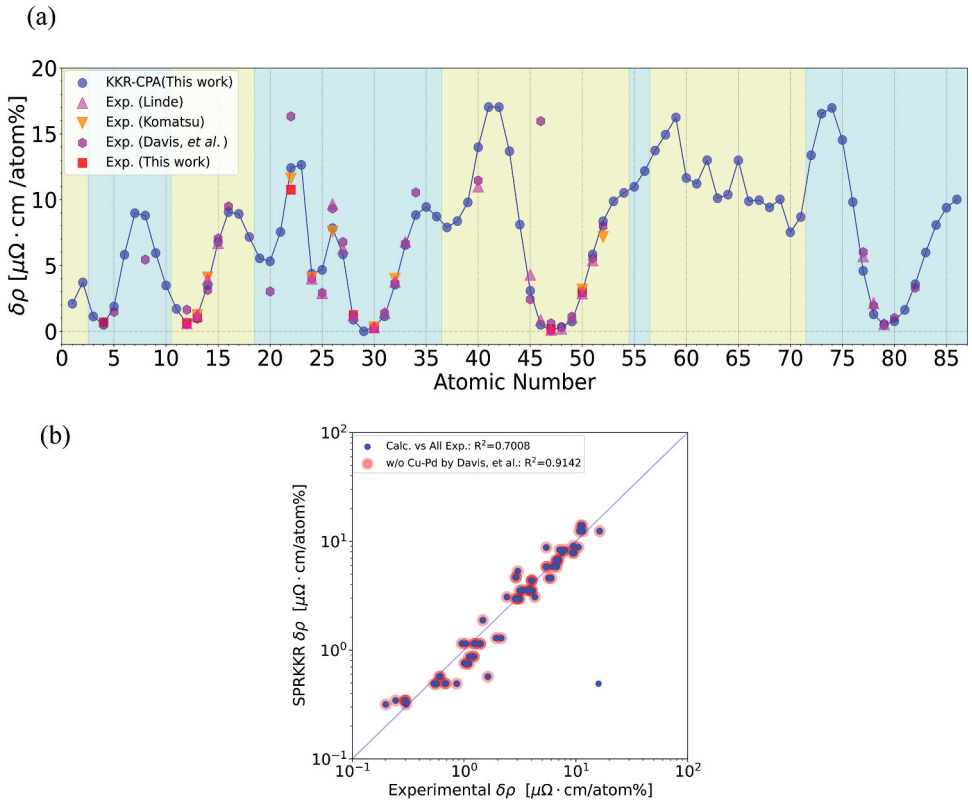

Figure 3. Calculated and experimental ERs of SS copper alloys. (a) ER increases relative to the pure Cu for solute elements of H to Rn obtained using first-principles calculations by KKR-CPA and experimental results obtained by Linde [35], Komatsu [36], Davis et al. [1], and those in this study. (b) Scatter plot of the experimental and calculated ERs with and without Cu–Pd data reported by Davis *et al.* [1].

and attempted to express the target by GPR as 'Model-2' with eight features $\mathbb{R}$, as described above. In features $\mathbb{R}$, we always used the feature $\log_{10}$(Model-1) with the parameters of Table 1 because we expected that the difference between the experimental values and Model-1 could be expressed by the mean values of molar fraction for the seven elemental features. Combinations of features, up to 7 were evaluated as depicted in Figure 4(b). Note that the RMSE was minimized by adding the minimum number of the features to $\log_{10}$(Model-1), *i.e.* only one, suggesting that overlearning is suppressed. The selected feature was the atomic mass that is a monotonically increasing quantity in the periodic table. The obtained results should provide a correction contribution that depends on the position in the periodic table. Hereafter, we define Model-2 for SSS as the obtained GPR with the two features.

$$(\sigma - \sigma_0)_{Model-2} \equiv 10^{Model-2} \tag{10}$$

As shown in Figure 4(c), not only the training set, but also the testing set of six data is predicted very well by Model-2 with a coefficient of determination $R^2 > 0.9$. This demonstrates the obtained Model-2 has high predictive performance.

Table 1. Optimal parameters of Model-1.

A	p	q	α
0.03790	0.7301	0.9169	9.533×10^3

3.4. Comprehensive elemental screening model for SS copper alloy

We define the figure-of-merit (FOM) formula as

$$\mathrm{FOM} \equiv \log_{10}\left[\frac{\sigma - \sigma_0}{(\rho - \rho)^q}\right] \tag{11}$$

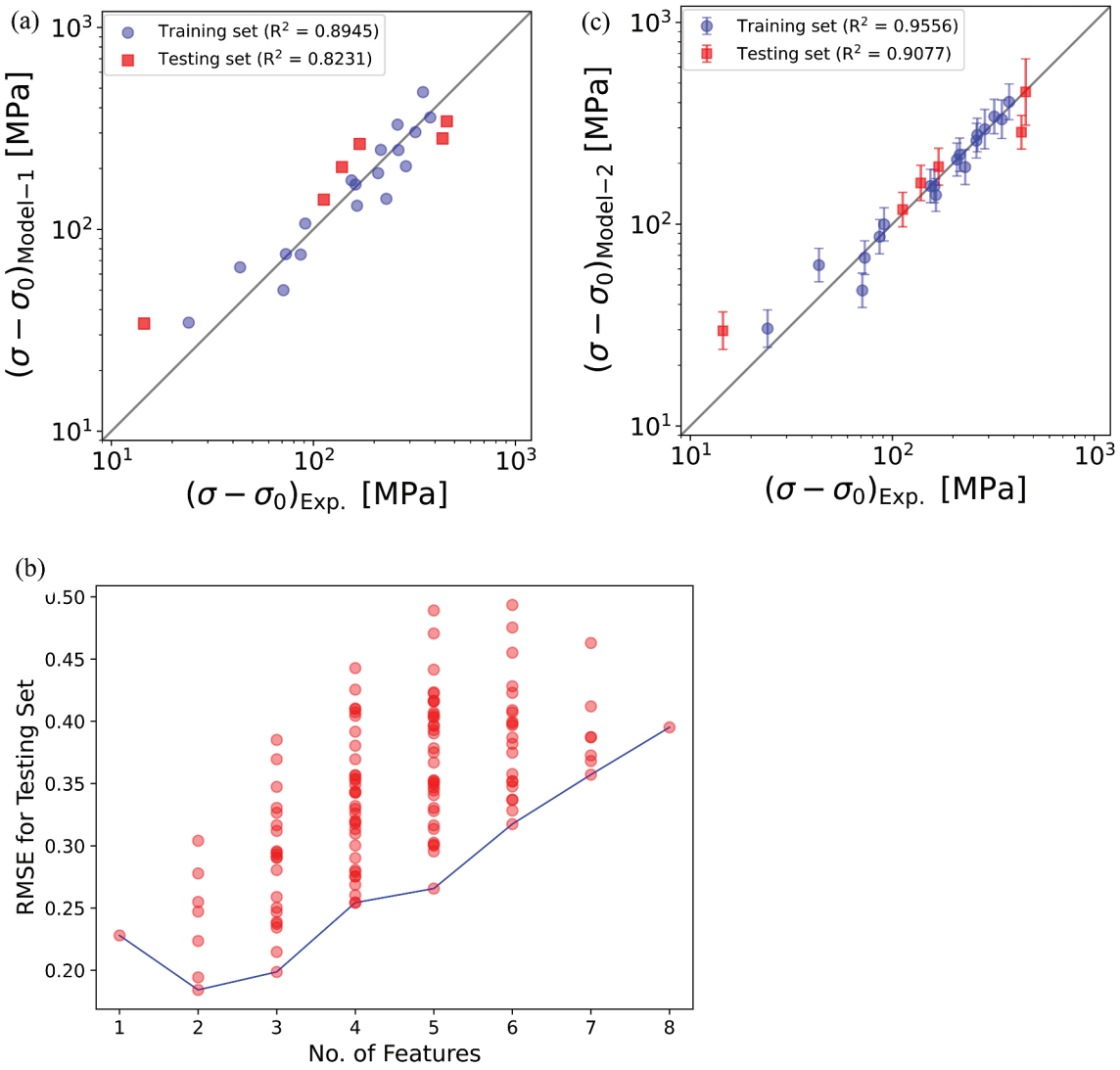

Figure 4. SSS modelling. (a) experimental vs. calculated (Model-1) SSS for the training and testing sets of CuX (X = Mg, Al, Ni, Zn, and Sn) and CuX (X = Be, Ti, and Ag), respectively. (b) number of selected features and RMSE for the testing set. 'No. of features' = 1 represents the model with the feature of $\log_{10}$(Model-1). The values of RMSE for 'no. of features' = *N* are evaluated by the feature of $\log_{10}$(Model-1) and combination of *N* −1 out of the seven elemental features. (c) experimental vs. predicted (Model-2) SSS for the training and testing sets of CuX (X = Mg, Al, Ni, Zn, and Sn) and CuX (X = Be, Ti, and Ag), respectively. The error bars are the standard deviations obtained via the prediction of GPR model.

FOM by Model-1 is independent on the molar fraction x,

$$\mathrm{FOM}_{\mathrm{Model-1}} \equiv \log_{10}\left[\frac{B_X}{\{\delta\rho(X)\}^q}\right] \quad (12)$$

according to Equations (7) and (8). At a larger FOM, the element X increases the effect of SSS more while suppressing the increase in the ER. Therefore, we propose that the FOM can be used for a comprehensive elemental screening for SS copper alloys. According to Equations (10) and (11), the FOM obtained using Model-2 is dependent of the molar fraction x. However, Equation (7) is a good approximation for low x values, and thus we define the FOM obtained by Model-2 at $x = 1.0$ atom%. The obtained FOMs vs. atomic number are presented in Figure 5(a). The results show a periodicity; local maxima exist at a number of valence electrons of 1 or 2, at the atomic numbers of the solution elements of Be, Mg, K, Rb, Ag, and Hg. It seems natural that an element without a significant difference in the number of valence electrons does not have a severe scattering effect on the ER compared to copper with valence electrons of 1. These elements have significant differences in the lattice constants, as shown in Figure 2. As a result, the FOMs are increased with the elements with valence electrons of 1 or 2. The FOM-1 results are replotted in the electrical resistivity increase $\delta\rho(X)$ (Equation (7)) vs. SSS factor B_X (Equation (8)) plane, as shown in Figure 5(b). Widely used SS elements, such as Zn, Sn, Al, Be, and Ni [1], are distributed around FOM = 1-2. The results suggest that the solution elements with FOM > 2 provide outstanding properties. Top 10 elements with regard to FOM are shown in Table 2 (for all results, see Supplementary material). Eight elements (Ag, Cd, In, Hg, Au, Tl, Mg, and Pb) are predicted in the top 10 for both Model-1 and Model-2. Among all elements of H to Rn, Ag is the best solute element according to both models. Cu–Ag is a high-performance but expensive alloy [1]. Despite its toxicity, Cu–Cd is also a high-performance copper alloy [1]. We reported that the Cu–Mg SS alloy exhibits excellent properties [2,3]. Recently, Cu–In was predicted and realized as a high-performance alloy [6], consistent with our model predictions. Regarding the practical application of Cu–In, we must be aware of the reported cancer risk of indium [37]. Cu–Au and Cu–Tl have not been reported in Ref. [1]; they are expensive and toxic, respectively. In addition, the solubility

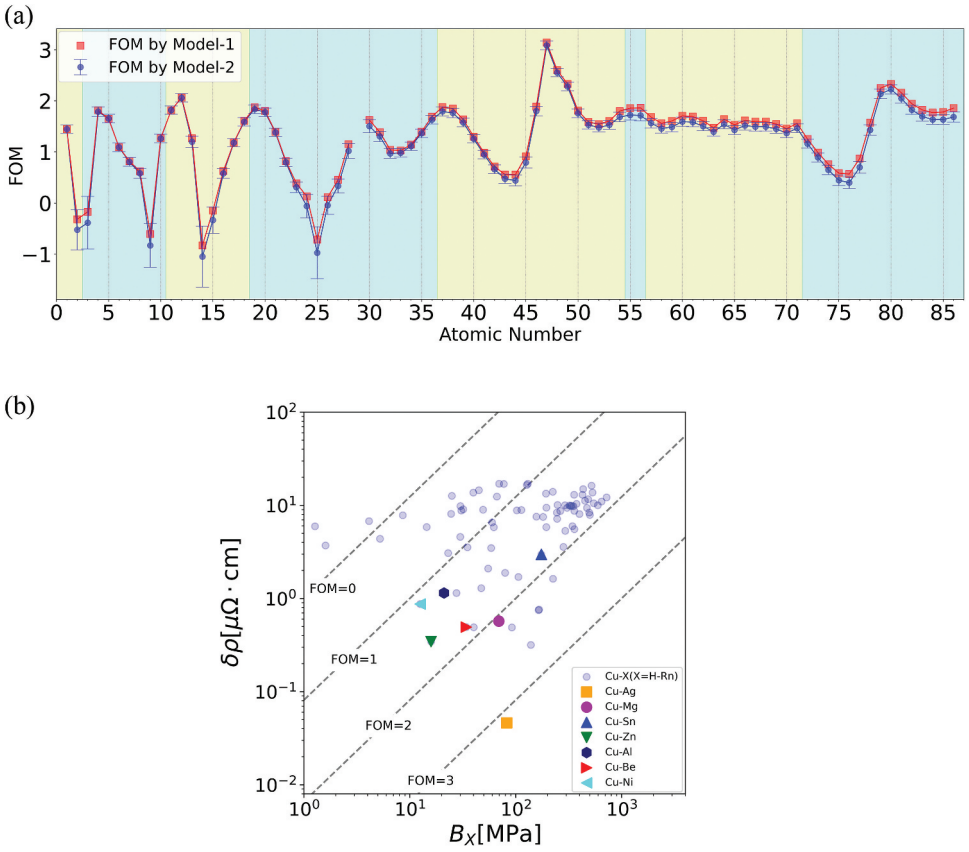

Figure 5. FOM of SS copper alloys. (a) FOM vs. atomic number as a comprehensive elemental screening model for SS copper alloys using Model-1 and Model-2. The error bars are the standard deviations obtained via the prediction of the GPR model for Model-2. (b) predicted results using Model-1 plotted in the electrical resistivity increase $\delta\rho(X)$ (Equation (7)) vs. SSS factor B_X (Equation (8)) plane.

Table 2. Top 10 elements of FOM by Model-1 and Model-2.

Element	$FOM_{Model\text{-}1}$	Element	$FOM_{Model\text{-}2}$
Ag	3.140	Ag	3.085
Cd	2.601	Cd	2.552
In	2.331	In	2.280
Hg	2.331	Hg	2.225
Au	2.249	Au	2.135
Tl	2.158	Mg	2.058
Mg	2.064	Tl	2.047
Pb	1.943	K	1.837
Pd	1.887	Pb	1.824
Rb	1.878	Na	1.818

limit in Cu–Tl is quite low [38]. The toxic Cu–Hg is also not presented in Ref. [1]. Although the nature of the periodic table suggests that our result is relatively natural, our prediction for Cu–Hg might be overestimated because of the large atomic size misfit, as shown in Figure 2. Cu–Pb is also a practical alloy [1]; however, Pb is used as an additive for free machining despite its toxicity. Cu–Pb is not considered as a high-performance copper SS alloy because of the low solubility limit of 0.09 atom% [38]. The increase in the ER of Cu–Pd could be overestimated in Ref. [1], as discussed above and as reported by Linde [35]. Although the element is comparatively expensive, further practical studies on Cu–Pd may be of significance. The other solution elements in Table 2, Na, K, and Rb, may also provide good results but have extremely low solid solution limits [38]. According to these results, our comprehensive elemental screening using both Model-1 and Model-2 would predict reasonable results. From economic, environmental, and healthcare perspectives, Cu–Mg is an appropriate choice according to the results in Table 2.

4. Conclusions

A comprehensive elemental screening framework was used to predict the SSS and ER of copper alloys. The ERs are predicted using first-principles calculations with KKR-CPA. We obtained a high degree of accuracy with $R^2 = 0.91$. Two models were considered to predict SSS. One of them was Model-1, with the generalized critical resolved shear stress formula. It provided a reasonable accuracy of $R^2 = 0.82$ for the testing set of our experimental data. The other was Model-2, which exhibited a high prediction performance of $R^2 > 0.9$ for the testing set. To construct Model-2, GPR with the features of mean atomic mass and $\log_{10}(\text{Model-1})$ was used. Combining the predicted ER and SSS, we established the FOM formula for the comprehensive elemental screening. The FOMs, obtained by both Model-1 and Model-2, provided reasonable results. The models predicted the already known Cu–Ag (Cd, In, Mg) as high-performance copper alloys. All solute elements including hypothetical copper alloys were ranked, and the less studied Cu–Hg (Tl, Au) were predicted to be high-performance structures. On the other hand, from economic, environmental, and healthcare perspectives, Cu–Mg is an appropriate choice among them.

Acknowledgements

This study was started in Mitsubishi Materials Corporation (MMC) and was carried out in the MMC- National Institute for Materials Science (NIMS) Center of Excellence for Materials Informatics Research. We also would like to thank Editage (http://www.editage.com) for English language editing.

Disclosure statement

No potential conflict of interest was reported by the author(s).

Funding

The work was supported by the Mitsubishi Materials Corporation.

Data availability statement

The data that support the findings of this study are available from the corresponding author upon reasonable request.

References

[1] Davis JR, editor. ASM specialty handbook: copper and copper alloys. Materials Park (OH): ASM International; 2001.
[2] Maki K, Ito Y, Matsunaga H, et al. Solid-solution copper alloys with high strength and high electrical conductivity. Scr Mater. 2013;68(10):777–780. doi: 10.1016/j.scriptamat.2012.12.027
[3] Ito Y, Matsunaga H, Mori H, et al. Effect of plastic deformation on the proof strength and electrical conductivity of copper-magnesium supersaturated solid-solution alloys. Mater Trans. 2014;55 (11):1738–1741. doi: 10.2320/matertrans.M2014220
[4] Liu X, Xu P, Zhao J, et al. Material machine learning for alloys: applications, challenges and perspectives. J Alloys Compd. 2022;921:165984. doi: 10.1016/j.jallcom.2022.165984
[5] Wang C, Fu H, Jiang L, et al. A property-oriented design strategy for high performance copper alloys via machine learning. NPJ Comput Mater. 2019;5 (1):57–64. doi: 10.1038/s41524-019-0227-7
[6] Zhang H, Fu H, He X, et al. Dramatically enhanced combination of ultimate tensile strength and electric conductivity of alloys via machine learning screening. Acta Mater. 2020;200:803–810. doi: 10.1016/j.actamat.2020.09.068
[7] The Materials Project [Internet]. Berkeley (CA): Berkeley LAB; [cited 2023 Apr 10]. Available from: https://materialsproject.org/

[8] AFLOW, Automatic-flow for Materials Discovery [Internet]. Durham (NC): Duke University; [cited 2023 Apr 10]. Available from: https://aflowlib.org/
[9] NOMAD, Novel materials discovery [Internet]. Berlin (Germany): NOMAD Lab; [cited 2023 Apr 10]. Available from: https://nomad-lab.eu/services/repo-arch
[10] Fleischer RL. Substitutional solution hardening. Acta Metall. 1963;11(3):203–209. doi: 10.1016/0001-6160(63)90213-X
[11] Labusch R. A statistical theory of solid solution hardening. Phys Status Solidi B. 1970;41(2):659–669. doi: 10.1002/pssb.19700410221
[12] Loibl A, Espinoza LAT. Current challenges in copper recycling: aligning insights from material flow analysis with technological research developments and industry issues in Europe and North America. Resour Conserv Recycl. 2021;169:105462. doi: 10.1016/j.resconrec.2021.105462
[13] Wesemann I, Hoffmann A, Mrotzek T, et al. Investigation of solid solution hardening in molybdenum alloys. Int J Refract Met Hard Mater. 2010;28(6):709–715. doi: 10.1016/j.ijrmhm.2010.05.010
[14] Walbrühl M, Linder D, Ågren J, et al. Modelling of solid solution strengthening in multicomponent alloys. Mater Sci Eng A. 2017;700:301–311. doi: 10.1016/j.msea.2017.06.001
[15] Blöchl PE. Projector augmented-wave method. Phys Rev B. 1994;50(24):17953–17979. doi: 10.1103/PhysRevB.50.17953
[16] Perdew JP, Burke K, Ernzerhof M. Generalized gradient approximation made simple. Phys Rev Lett. 1996;77(18):3865–3868. doi: 10.1103/PhysRevLett.77.3865
[17] Kresse G, Hafner J. Ab initio molecular dynamics for liquid metals. Phys Rev B. 1993;47(1):558–561. doi: 10.1103/PhysRevB.47.558
[18] Kresse G, Hafner J. Ab initio molecular-dynamics simulation of the liquid-metal amorphous- semiconductor transition in Germanium. Phys Rev B. 1994;49:14251–14269. doi: 10.1103/PhysRevB.49.14251
[19] Kresse G, Furthmüller J. Efficiency of Ab-initio total energy calculations for metals and semiconductors using a plane-wave basis set. Comput Mater Sci. 1996;6(1):15–50. doi: 10.1016/0927-0256(96)00008-0
[20] Kresse G, Furthmüller J. Efficient iterative schemes for Ab initio total-energy calculations using a plane-wave basis set. Phys Rev B. 1996;54(16):11169–11186. doi: 10.1103/PhysRevB.54.11169
[21] Kresse G, Joubert D. From ultrasoft pseudopotentials to the projector augmented-wave method. Phys Rev B. 1999;59(3):1758–1775. doi: 10.1103/PhysRevB.59.1758
[22] Chung DH. Elastic moduli of single crystal and polycrystalline MgO. Phil Mag. 1963;8(89):833–841. doi: 10.1080/14786436308213840
[23] King HW. Quantitative size-factors for metallic solid solutions. J Mater Sci. 1966;1(1):79–90. doi: 10.1007/BF00549722
[24] Korringa J. On the calculation of the energy of a Bloch wave in a metal. Physica. 1947;13(6–7):392–400. doi: 10.1016/0031-8914(47)90013-X
[25] Kohn W, Rostoker N. Solution of the Schrödinger equation in periodic lattices with an application to metallic lithium. Phys Rev. 1954;94(5):1111–1120. doi: 10.1103/PhysRev.94.1111
[26] Soven P. Coherent-potential model of substitutional disordered alloys. Phys Rev. 1967;156(3):809–813. doi: 10.1103/PhysRev.156.809
[27] Ebert H, et al. The Munich SPR-KKR package. Available from: http://ebert.cup.uni-muenchen.de/SPRKKR
[28] Ebert H, Ködderitzsch D, Minár J. Calculating condensed matter properties using the KKR-Green's function method—recent developments and applications. Rep Prog Phys. 2011;74(9):096501. doi: 10.1088/0034-4885/74/9/096501
[29] Tulip PR, Staunton JB, Lowitzer S, et al. Theory of electronic transport in random alloys with short-range order: Korringa-Kohn-Rostoker nonlocal coherent potential approximation. Phys Rev B. 2008;77(16):165116. doi: 10.1103/PhysRevB.77.165116
[30] Ebert H, Mankovsky S, Chadova K, et al. Calculating linear-response functions for finite temperatures on the basis of the alloy analogy model. Phys Rev B. 2015;91(16):165132. doi: 10.1103/PhysRevB.91.165132
[31] Tran F, Laskowski R, Blaha P, et al. Performance on molecules, surfaces, and solids of the Wu–Cohen GGA exchange–correlation energy functional. Phys Rev B. 2007;75:115131. doi: 10.1103/PhysRevB.75.115131
[32] Ong SP, Richards WD, Jain A, et al. Python Materials genomics (pymatgen): a robust, open-source python library for materials analysis. Comput Mater Sci. 2013;68:314–319. doi: 10.1016/j.commatsci.2012.10.028
[33] Pedregosa F, Varoquaux G, Gramfort A, et al. Scikit-learn: machine learning in Python. J Mach Learn Res. 2011;12:2825–2830.
[34] Ward L, Dunn A, Faghaninia A, et al. Matminer: an open source toolkit for materials data mining. Comput Mater Sci. 2018;152:60–69. doi: 10.1016/j.commatsci.2018.05.018
[35] Linde JO. An experimental study of the resistivity-concentration dependence of alloys. Helv Phys Acta. 1968;41:1007–1015.
[36] Komatsu S. Resistivity of copper alloys, its interpretation and application. J Jpn Res Inst Adv Copper-Base Mater Tech. 2002;41:1–9. Japanese.
[37] Nakano M, Omae K, Tanaka A, et al. Possibility of lung cancer risk in indium-exposed workers: an 11-year multicenter cohort study. J Occup Health. 2019;61(3):251–256. doi: 10.1002/1348-9585.12050
[38] Massalski TB, editor. Binary alloy phase diagrams. 2nd ed. Materials Park (OH): ASM International; 1990.